Talanta 161 (2016) 567–573

Contents lists available at ScienceDirect

Talanta

journal homepage: www.elsevier.com/locate/talanta

A highly selective electrochemical sensor for chloramphenicol based on three-dimensional reduced graphene oxide architectures

Xuan Zhang *, Yi-Chi Zhang, Jia-Wei Zhang

College of Chemistry, Chemical Engineering & Biotechnology, Donghua University, Shanghai 201620, China

ARTICLE INFO

Article history:
Received 5 June 2016
Received in revised form
1 September 2016
Accepted 3 September 2016
Available online 4 September 2016

Keywords:
Three-dimensional reduced graphene oxide
Electrochemical sensor
Metal-free electrocatalyst
Chloramphenicol

ABSTRACT

Chloramphenicol (CAP), as a broad-spectrum antibiotic, has been worldwide banned for using in the food producing animals due to its overuse may cause severe threats to public health. It is therefore highly desirable to develop facile, selective and sensitive biosensor for CAP detection and monitoring in drug and foodstuff samples. In this work, three-dimensional reduced graphene oxide (3DRGO) architectures were prepared through a green and template-free approach and used as active electrode materials to develop a highly selective electrochemical sensor for CAP detection. The spontaneous reduction and assembly of graphene oxide via zinc foil was completed at room temperature, followed by washing with diluted hydrogen chloride solution, to produce 3DRGO. The as-prepared 3DRGO were characterized by scanning electron microscopy (SEM), transmission electron microscope (TEM), X-ray diffraction (XRD), X-ray photoelectron spectroscopy (XPS) and Raman spectroscopy. An electrochemical biosensor for CAP was constructed based on 3DRGO-modified glass carbon electrode (3DRGO/GCE). It was revealed that the present 3DRGO/GCE sensor exhibited a remarkable performance with a detection range of 1–113 μmol L^{-1} and a detection limit of 0.15 μmol L^{-1} at physiological pH 7.4. Moreover, the sensor showed an excellent selectivity, stability, reproducibility, and satisfying recovery result for CAP detection in real samples.

1. Introduction

As a new class of nanocarbon material, graphene has attracted tremendous attention due to its excellent properties such as extraordinary electrical conductivity, fast electron transfer kinetics, high surface area and remarkable mechanical strength [1–3]. These features make graphene a promising electrode material for various applications, such as electrochemical sensing, catalysis and energy storage [4–8]. However, when used as an electrode material, two-dimensional graphene usually exhibits a dramatically decreased surface area that hindered the practical application, because these graphene nanosheets tend to stack and form agglomerates [9]. To increase the accessible surface area of graphene material and facilitate its practical applications, many efforts have been devoted to construct three-dimensional (3D) graphene materials [10–16]. Recently, 3D graphene architectures have been successfully fabricated by various methods such as self-assembly, template-assisted synthesis as well as chemical vapor deposition (CVD) [17–21]. For example, 3D layered graphene architectures have been achieved via an ordered self-assembly process by using cross-linking agent of poly(vinyl alcohol) [22]. Yu et al. have prepared 3D graphene electrode materials by polystyrene-spheres-templated approach that showed an enhanced sensitivity for dopamine detection [23]. Kota et al. have reported the fabrication of ice-templated 3D graphene material and achieved excellent supercapacitive performances [24]. 3D graphene nanostructures have also been synthesized through CVD by using porous nickel foam as a substrate, and used to construct a dopamine biosensor that exhibited remarkably improved sensing performance [25]. Although the 3D graphene nanostructures have been emerged as promising materials for various applications, the complicate construction conditions and additional templates are usually involved. Therefore, the development of simple and green methods for 3D graphene architectures fabrication is still a challenging task.

Chloramphenicol (CAP), a broad-spectrum antibiotic that is effective against to a wide variety of bacteria, has been extensively used since the 1950s for the treatment of infectious diseases in both humans and animals [26–28]. However, the overuse of antibiotics would result in accumulation of antibiotics in food and water that may cause severe threats to public health [28]. For example, it has been known that the CAP may cause bone marrow depression, aplastic anemia, cardiovascular collapse, etc. [26–29]. Thus the use of CAP in the food producing animals has been worldwide banned in recent years. But the fact is that CAP is still illegally used in cows to control mastitis and other animal diseases

* Corresponding author.
E-mail address: xzhang@dhu.edu.cn (X. Zhang).

http://dx.doi.org/10.1016/j.talanta.2016.09.013
0039-9140/

because of its low cost and high effectiveness [30]. Therefore, it is highly desirable to develop facile, selective and sensitive analytical methods for CAP detection and monitoring in drug and foodstuff samples.

Various analytical methods, such as liquid chromatography (LC) [31], gas chromatography (GC) [32], LC-mass spectrometry (LC-MS) [33], GC–MS [34], electrophoresis [35], Raman scattering [36], and chemiluminescence [37], have been developed for CAP detection. Nevertheless, the requirements for complicated analytical procedures, expensive instruments, tedious separation steps limit the extensive routine applications of these methods. Alternatively, electrochemical method for CAP detection offers the advantages of fast analysis, good sensitivity, simple operation, and low cost [38–40]. In this regard, various electrode materials, such as self-doped polyaniline intercalated molybdenum disulfide [41], nitrogen-doped graphene nanosheets decorated with gold nanoparticles [42], titanium nitride–reduced graphene oxide nanohybrids [43], magnetic hollow porous nanoparticles [44], silver nanoparticles/sulfonated functionalized graphene [45], and 1,5-diaminonaphthalene polymer modified aptamer [46], have been employed for determination of CAP. Most of these reported electrode materials either require complicated preparation processes or show poor sensitivity, and therefore the electrochemical sensing performances still need to be improved for a practical application.

Here we will report a facile preparation of three-dimensional reduced graphene oxide (3DRGO) architecture via green and template-free approach, and its application in construction of electrochemical biosensor for CAP. The as-prepared 3DRGO materials were fully characterized and their sensing performance was investigated by electrochemical determination of CAP, which showed an excellent selectivity, stability, reproducibility, and satisfying recovery result for CAP detection in real samples.

2. Experimental

Graphite powder was obtained from XFNano (99.9%, Nanjing, China). Chloramphenicol was provided by Amresco (AR, USA). All other chemicals were purchased from Sinopharm (AR, Shanghai, China) and used as received. Phosphate buffered saline (PBS, pH=7.4) was prepared from Na_2HPO_4 (0.1 mol L^{-1}) and KH_2PO_4 (0.1 mol L^{-1}), containing NaCl (0.1 mol L^{-1}) and KCl (0.01 mol L^{-1}).

2.1. Preparation of 3DRGO electrode

The 3DRGO was prepared through spontaneous reduction of graphene oxide via zinc foil at room temperature [14,47]. Briefly, graphene oxide (GO) was firstly produced from graphite powder according to the modified Hummers method [48,49]. The Zn foil was then immersed into an aqueous GO suspension (0.5 mg mL^{-1}, 30 mL) for 7 h without any additives at room temperature. The black deposition formed on Zn foil surface was collected by ultrasonication, cleaned by sinking the graphene materials into diluted HCl under stirring for 30 min. The solid was then collected by centrifugation and washed with water for three times, and finally dried in vacuum at 40 °C overnight to afford the 3DRGO architectures. 3DRGO was then dispersed in ethanol (2.0 mg mL^{-1}) and 3 μL of suspension was transferred on the pre-polished glassy carbon electrode (GCE) to construct the 3DRGO/GCE electrodes. For a comparison, normally reduced graphene oxide (N-RGO) was also prepared by using hydrazine hydrate based on reported procedure [42], and used to similarly construct the N-RGO/GCE electrodes.

2.2. Characterization

Scanning electron microscopy (SEM) and transmission electron microscopy (TEM) were completed on S-4800 (Hitachi, Japan) and JEM-2100F (JEOL, Japan), respectively. X-ray diffraction (XRD) and X-ray photoelectron spectroscopy (XPS) were recorded on D/max 2550 (Rigaku, Japan) and PHI 5400 (PE, USA), respectively. Raman spectrum was measured on inVia-Reflex (Renishaw, UK). Electrochemical measurements were conducted on CHI-660D electrochemical workstation (Shanghai Chenhua, China) with a common three-electrode system, including GCE or graphene modified GCE as working electrode, Pt wire and saturated calomel electrode (SCE) as counter and reference electrodes, respectively. The cyclic voltammetry (CV) performed from –0.2 to 0.6 V or –1 to 1 V (vs. SCE) with the scan rate of 50 mV s^{-1}. The differential pulse voltammetry (DPV) was carried out in 0.1 mol L^{-1} PBS +0.1 mol L^{-1} KCl at pH 7.4 from −0.4 to −0.7 V (vs. SCE), with step potential of 4 mV, amplitude of 50 mV, pulse width of 0.2 s and pulse period of 0.5 s, respectively. Electrochemical impedance spectroscopy (EIS) was recorded in 0.1 mol L^{-1} KCl solution containing 5 mmol L^{-1} $K_3[Fe(CN)_6]$, where the frequency range is from 0.01 Hz to100 kHz with a signal amplitude of 5 mV and the scan rate of 100 mV s^{-1}. All electrochemical measurements were carried out under nitrogen atmosphere at room temperature.

3. Results and discussion

3.1. Characterization of 3DRGO

The as-prepared 3DRGO materials were characterized by SEM, TEM, XPS, XRD and Raman spectra, respectively. As shown in Fig. 1, porous 3D architectures with obvious ripples and wrinkles on the graphene surface have been revealed by SEM and TEM

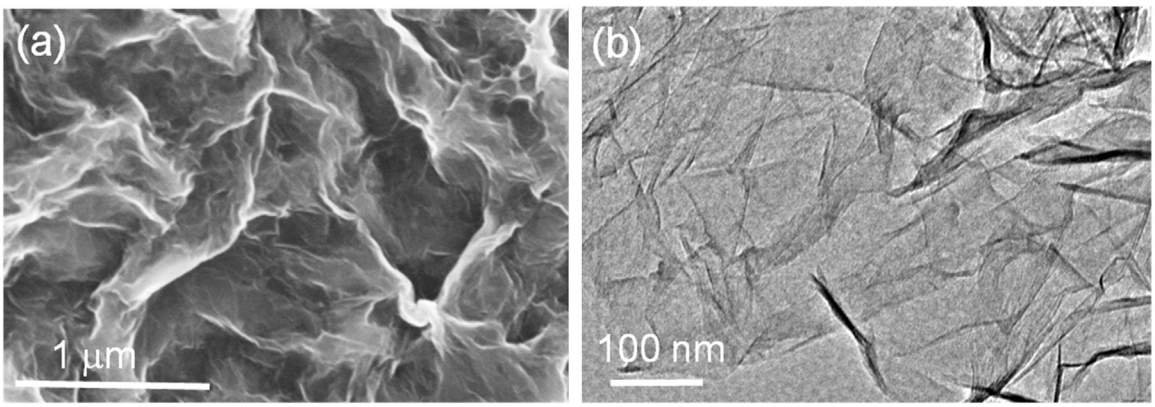

Fig. 1. SEM (a) and TEM (b) images of 3DRGO materials.

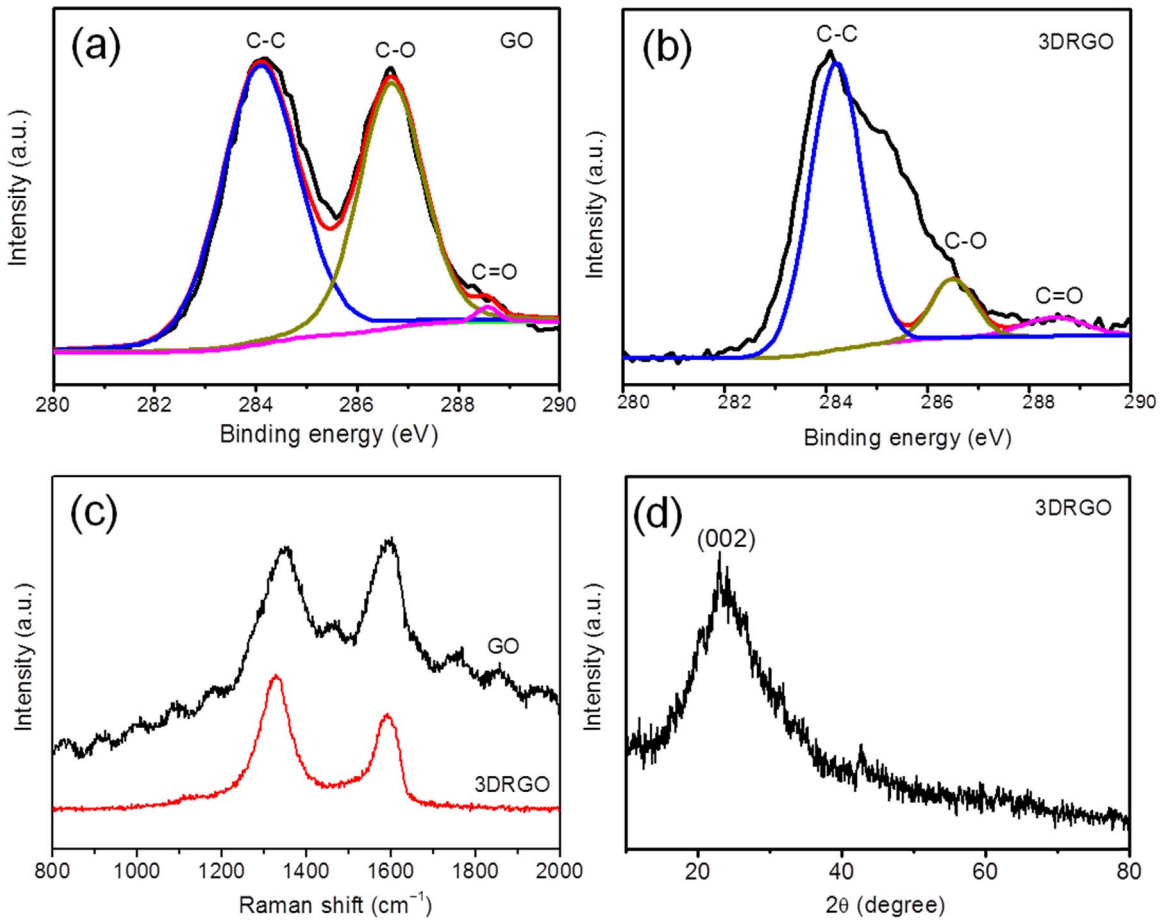

Fig. 2. XPS (a, b), Raman spectra (c) and XRD pattern (d) of GO and 3DRGO, respectively.

observations. The reduction of GO was confirmed by XPS analysis as shown in Fig. 2. It was noted that the C 1 s XPS of GO and 3DRGO were fitted into three peaks centered at 284.6, 286.8, 288.5 eV, attributing to the C–C/C=C in alkyl and sp^2-bonded carbon network, the C-O in hydroxyl and epoxy groups, and the C=O in carbonyl and ketone, respectively (Fig. 2a and b) [49]. Obviously, the C–O and C=O peak intensity remarkably weakened in 3DRGO, and the C–C/C–O peak intensity ratio is 2.4 in the 3DRGO, much higher than that in GO (1.1). These indicate that the oxygen containing groups were largely removed and GO was mainly reduced to graphene by Zn foil. Raman spectra of GO and 3DRGO exhibits two intense peaks, one is the G band (1592 cm^{-1}) and the other one is the D-band (1320 cm^{-1}) (Fig. 2c). The higher intensity ratio of the D to G peak (I_D/I_G) in 3DRGO (1.36) than in GO (0.96) proves the increase of sp^2 carbon in the former due to reduction [50]. The XRD spectrum showed a broad peak around $2\theta=24°$ (Fig. 2d), corresponding to an interlayer distance of 0.36 nm of reduced graphene oxide sheets [50]. These results indicate that the 3DRGO architectures were successfully fabricated by Zn foil spontaneous reduction induced self-assembly.

3.2. Electrochemical characterization of 3DRGO electrode

The electrochemical performances of various electrodes were firstly investigated by CV with $K_3[Fe(CN)_6]$ as redox probe. The CV curves of 0.5 mmol L^{-1} $K_3[Fe(CN)_6]$ containing 0.1 mol L^{-1} KCl on the GCE, N-RGO/GCE and 3DRGO/GCE were displayed in Fig. 3a, respectively. Although a pair of well-defined redox peaks was observed on all of these electrodes, the current intensity was followed the order of 3DRGO/GCE > N-RGO/GCE > GCE, revealing that 3DRGO electrode materials own the best activity, probably due to their 3D architectures provide the larger electroactive surface area (EASA). The EASA was then estimated by the peak current intensity (*Ip*) according to the following Randles-Sevcik equation (25 °C) [51,52].

$Ip = 2.69 \times 10^5 \times n^{3/2} AD^{1/2}v^{1/2}C$ where n is the number of electrons take part in the redox reaction (n=1 for one-electron transfer reaction), A is the electroactive surface area (in cm^2), D is the diffusion coefficient ($D=6.50 \times 10^{-6}$ cm^2 s^{-1}) [53], C is the bulk concentration (in mol cm^{-3}), v is the scan rate (in V s^{-1}). The effective EASA of 3DRGO/GCE was estimated to be 0.22 cm^2, which is larger than those of N-RGO/GCE (0.17 cm^2) and the bare GCE (0.05 cm^2). The larger EASA of graphene modified electrodes can be attributed to the high surface area of graphene nanomaterials, whereas the largest EASA of 3DRGO/GCE could be related to its more porous 3D structure than that of N-RGO [42]. EIS has been known to be a powerful technique to reveal detailed information on the impedance changes of electrodes, where the semicircle in impedance spectra at higher frequencies corresponds to the electron-transfer limited process, and the linear portion at lower frequencies represents the diffusion-limited process [53]. As shown in Fig. 3b, very small semicircle domains were observed on graphene modified electrodes, 3DRGO/GCE and N-RGO/GCE, implying their very low electron-transfer resistance [53]. Both the larger electroactive surface area and lower electron-transfer resistance suggest that the 3DRGO/GCE can serve as a promising platform for electrochemical sensor construction.

The electrochemical behaviors of CAP on various electrodes were then investigated by CV and DPV. As shown in Fig. 3c, there are one oxidation peak at –131 mV and two reduction peaks at –

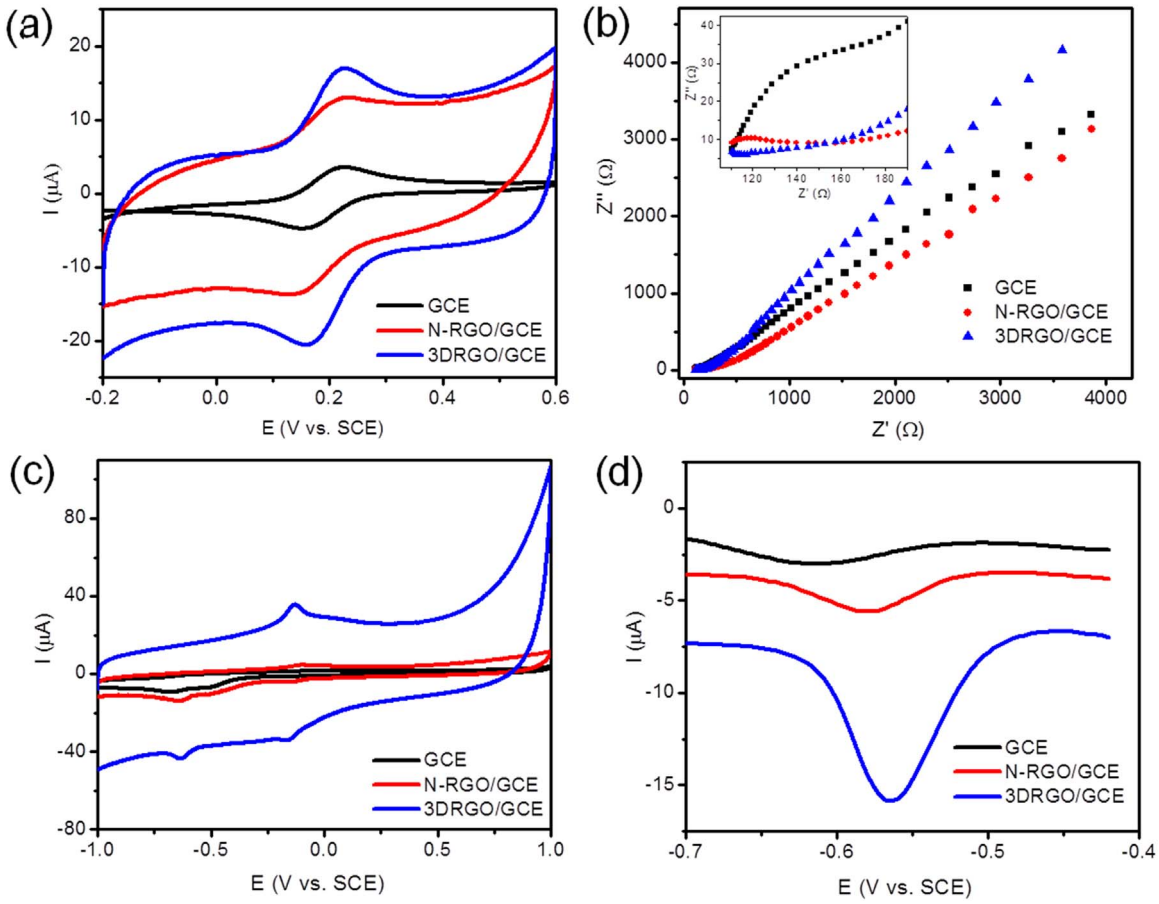

Fig. 3. CV curves of 0.5 mmol L^{-1} $K_3[Fe(CN)_6]$ (a), CV (c) and DPV (d) curves of 50 μmol L^{-1} CAP in 0.1 mol L^{-1} PBS solution (pH = 7.4) on bare GCE, N-RGO/GCE and 3DRGO/GCE, respectively. Nyquist plots (b) of these electrodes recorded in 0.1 mol L^{-1} KCl solution containing 5 mmol L^{-1} $K_3[Fe(CN)_6]$. The inset in (b) is the corresponding plots at higher frequency region.

170 and –633 mV respectively. These redox behaviors could be explained by considering the oxidation/reduction reactions of CAP, where the peak at –633 mV could be attributed to the irreversible reduction of the nitro group in CAP, and the other couple redox peaks were ascribed to the reversible redox of the intermediate hydroxylamine group [38,42]. The highest current intensity was observed on 3DRGO/GCE from both CV and DPV curves (Fig. 3c and d), revealing that 3DRGO materials could provide an excellent electrochemical sensing platform for CAP detection.

3.3. *Electrochemical performance of 3DRGO-based sensor for CAP detection*

To achieve a sensitive detection of CAP, the experimental conditions including the amounts of 3DRGO and pH were systematically optimized. As shown in Fig. 4a, the current intensity at –633 mV increased with increasing the volume of 3DRGO suspension (2.0 mg mL^{-1}) dropped on the GCE surface up to 3 μL, and significantly decreased with further increasing the volume of 3DRGO (Fig. 4b). This indicates the employment of 3DRGO can effectively increase the surface area of electrode, but excess 3DRGO could stack to thicker layers that hinder the electrical conductivity of material. Accordingly, the optimal amount of 3DRGO suspension solution was selected as 3 μL in this work. Fig. 4c showed the DPV behavior of CAP on 3DRGO/GCE in various pH values. With changing pH from 4 to 9, it can be seen that the peak potentials monotonically shifted to positive window, whereas the peak current increased firstly and reached the maximum at pH 7.4, and then significantly declined after that (Fig. 4d). The pH-dependent peak potential manifested that the proton involved in the redox reaction process. Taking the sensitivity and biocompatibility into account, the PBS buffer solution with physiological pH 7.4 was chosen for the further study.

To ascertain the mechanism of the reaction taken place on the 3DRGO/GCE, the kinetics of electrode reaction was studied by examining the influence of scan rate on the redox peak current and potential. As shown in Fig. 5, the redox current increased with increasing the scan rate (10–100 mV s^{-1}), and the peak intensities at –131, –170 and –633 mV are found to show quite good linear relationships with the scan rates, respectively. This implies that the redox of CAP on the 3DRGO/GCE is an adsorption controlled process [54].

Under the optimum experimental conditions, the linear detection range and detection limit of the as-prepared 3DRGO/GCE biosensor were obtained by DPV measurements in pH 7.4 PBS upon successive addition of CAP solutions (Fig. 6a). To make sure that the added CAP was fully mixed, the electrolyte solution was stirred for about 30 s before the DPV measurements. It is found that the reduction peak current at –633 mV gradually increased and was proportional to the CAP concentrations over the range of 1–330 μmol L^{-1} (Fig. 6a and b). The regression equations is expressed as I (μA) = $-0.1054C_{CAP}$ (μmol L^{-1}) – 8.5313 (R^2 = 0.9978). The detection limits for CAP is estimated to be 0.15 μmol L^{-1} (S/N = 3). By comparison with the previous reported electrochemical sensor towards CAP detection [41–43,45,55], the present 3DRGO/GCE showed a comparable or even better performance. Notably, metal nanoparticles or/and polymers were required for these previous electrodes, but the present sensor only employed 3DRGO

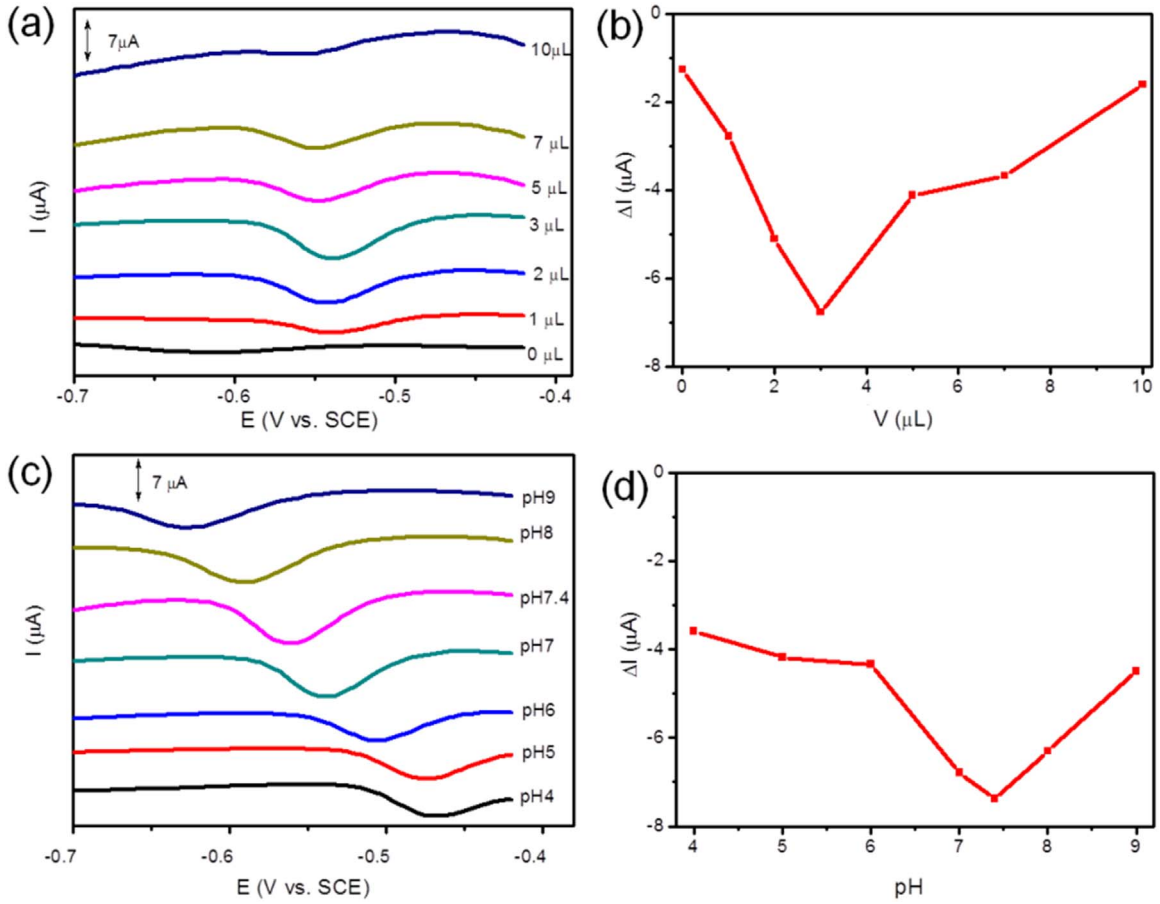

Fig. 4. DPV curves of CAP (50 μmol L^{-1}) on 3DRGO/GCE at various amounts of 3DRGO solution (a) and pH (c), and the corresponding peak current intensity versus the volume of 3DRGO solution (b) and pH (d).

architectures as metal-free electrode materials. This allows that the 3DRGO/GCE can serve as a potential electrochemical biosensor for CAP detection in real samples.

3.4. Reproducibility, stability, interference study and real sample analysis

The reproducibility and stability of 3DRGO/GCE was further tested. It was found that the measurements of 50 μmol L^{-1} CAP by independently-fabricated five electrodes showed an excellent reproducibility with the relative standard deviation (RSD) of 0.85%. The storage stability of the 3DRGO/GCE was investigated by exposing the electrode into air and monitoring the peak current change of 50 μmol L^{-1} CAP and the peak current remained almost no change after 30 days, indicating a good stability of 3DRGO/GCE. Moreover, the selectivity of 3DRGO/GCE towards CAP detection was investigated in the presence of various interfering species. It was found that the existence of 10 mmol L^{-1} KCl and NaCl,

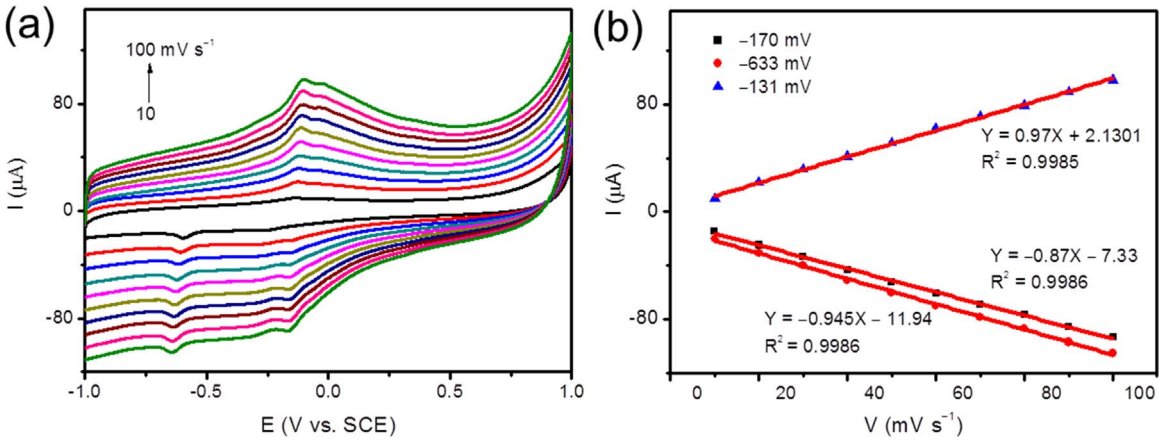

Fig. 5. CV curves of CAP (50 μmol L^{-1}) on 3DRGO/GCE in 0.1 mol L^{-1} PBS (pH = 7.4) with various scan rates (a) and the linear relationship between corresponding peak current intensity and scan rate (b).

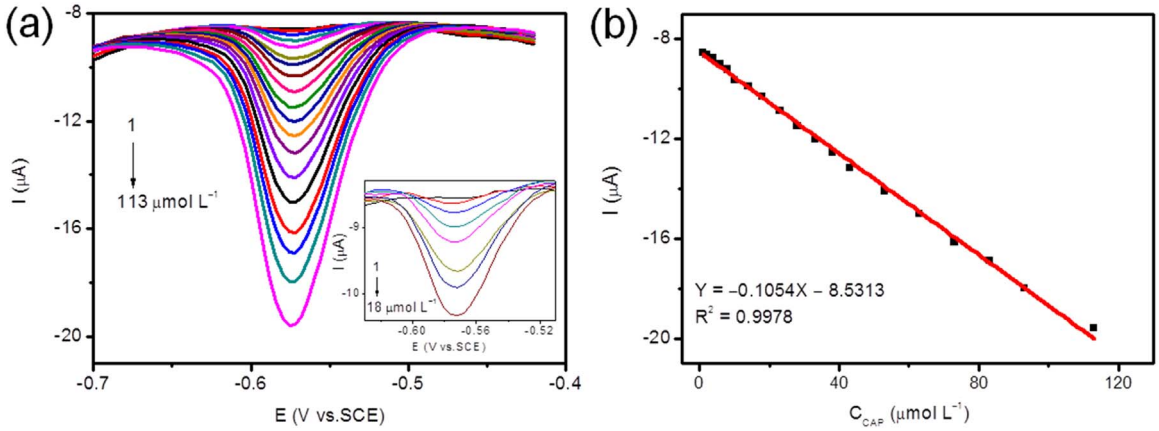

Fig. 6. DPV curves of various CAP concentrations on 3DRGO/GCE (a) and the calibration plots between peak current intensity and CAP concentration (b). The inset in (a) is the magnified DPV response at low concentration.

Table 1
Spike recovery results of CAP in real samples.

Samples	Added (μmol L^{-1})	Found (μmol L^{-1}, n=3)	Recovery (%)
CAP eye drops	0	26.01[a] ± 0.8	–
	5	31.24 ± 0.3	104.6
Milk	10	9.73 ± 1.2	97.3
	50	49.21 ± 0.2	98.4

[a] Given concentration is 25.79 μmol L^{-1} by manufacturer.

2 mmol L^{-1} glucose, 1 mmol L^{-1} cysteine, glutathione, taurine, $CaCl_2$, $MgSO_4$, $FeCl_3$, $CuSO_4$, and $ZnCl_2$, and 0.5 mmol L^{-1} uric acid does not interfere the detection of 50 μmol L^{-1} CAP (signal change below 5%). This suggests that the present 3DRGO/GCE exhibited excellent anti-interference ability, reproducibility and stability.

The application potential of 3DRGO/GCE on CAP detection was evaluated with the real chloramphenicol eye drops and milk samples, and the accuracy was estimated by using the standard addition method. All samples for DPV measurements were diluted 300 times with 0.1 mol L^{-1} PBS (pH=7.4) solution and the results are summarized in Table 1. It was noted that the recovery rates for CAP in these samples ranged from 97.3% to 104.6% respectively and the RSDs are lower than 5%. The concentration of CAP in eye drops is found to be 26.01 μmol L^{-1} that is very close to the value of 25.79 μmol L^{-1} given by manufacturer. These results indicate that the present 3DRGO/GCE is a promising electrochemical sensor for the practical detection of CAP.

4. Conclusions

Three-dimensional reduced graphene oxide (3DRGO) architectures were facilely prepared by a spontaneous reduction induced self-assembly of graphene oxide via zinc foil at room temperature. The as-prepared 3DRGO materials were developed as novel metal-free electrode materials for chloramphenicol (CAP) detection. The present 3DRGO/GCE sensor showed the largely increased electroactive surface area, lower electro-transfer resistance and enhanced sensitivity towards CAP detection at physiological pH 7.4. Furthermore, the biosensor exhibited excellent anti-interference ability, reproducibility, stability, and displayed a wide linear detection range, low detection limit and satisfying recovery result in real sample analysis. The fabrication of the present biosensor is simple, fast but effective to CAP detection that would contribute to develop advanced graphene-based interfacial electrode materials for electrochemical sensing.

Acknowledgment

This work was financially supported by Shanghai Municipal Natural Science Foundation (16ZR1401700) and Fundamental Research Funds for the Central Universities (No. 2232014D3-11).

References

[1] K.S. Novoselov, A.K. Geim, S.V. Morozov, D. Jiang, Y. Zhang, S.V. Dubonos, I. V. Grigorieva, A.A. Firsov, Electric field effect in atomically thin carbon films, Science 306 (2004) 666.
[2] Y. Zhu, S. Murali, W. Cai, X. Li, J.W. Suk, J.R. Potts, R.S. Ruoff, Graphene and graphene oxide: synthesis, properties, and applications, Adv. Mater. 22 (2010) 3906.
[3] Z. Li, Z. Liu, H. Sun, C. Gao, Superstructured assembly of nanocarbons: fullerenes, nanotubes,and graphene, Chem. Rev. 115 (2015) 7046.
[4] X. Huang, Z. Zeng, Z. Fan, J. Liu, H. Zhang, Graphene-based electrodes, Adv. Mater. 24 (2012) 5979.
[5] S.J. Guo, S.J. Dong, Graphene nanosheet: synthesis, molecular engineering, thin film, hybrids, and energy and analytical applications, Chem. Soc. Rev. 40 (2011) 2644.
[6] H. Wang, X. Yuan, G. Zeng, Y. Wu, Y. Liu, Q. Jiang, S. Gu, Three dimensional graphene based materials: synthesis and applications from energy storage and conversion to electrochemical sensor and environmental remediation, Adv. Colloid Interface 221 (2015) 41.
[7] T. Wu, M. Chen, L. Zhang, X. Xu, Y. Liu, J. Yan, W. Wang, J. Gao, Three-dimensional graphene-based aerogels prepared by a self-assembly process and its excellent catalytic and absorbing performance, J. Mater. Chem. A 1 (2013) 7612.
[8] Y. Xu, G. Shi, X. Duan, Self-assembled three-dimensional graphene macrostructures: synthesis and applications in supercapacitors, Acc. Chem. Res. 48 (2015) 1666.
[9] H.J. Qiu, Y. Guan, P. Luo, Y. Wang, Recent advance in fabricating monolithic 3D porous graphene and their applications in biosensing and biofuel cells, Biosens. Bioelectron. (2016), http://dx.doi.org/10.1016/j.bios.2015.12.029.
[10] C. Li, G. Shi, Three-dimensional graphene architectures, Nanoscale 4 (2012) 5549.
[11] H. Gao, H. Duan, 2D and 3D graphene materials: preparation and bioelectrochemical applications, Biosens. Bioelectron. 65 (2015) 404.
(12) X. Cao, Z. Yin, H. Zhang, Three-dimensional graphene materials: preparation, structures and application in supercapacitors, Energy Environ. Sci. 7 (2014) 1850.
[13] L.L. Jiang, Z.J. Fan, Design of advanced porous graphene materials: from graphene nanomesh to 3D architectures, Nanoscale 6 (2014) 1922.
[14] C. Hu, X. Zhai, L. Liu, Y. Zhao, L. Jiang, L. Qu, Spontaneous reduction and assembly of graphene oxide into three-dimensional graphene network on arbitrary conductive substrates, Sci. Rep. 3 (2013) 2065.
[15] J. Liu, X. Wang, T. Wang, D. Li, F. Xi, J. Wang, E. Wang, Functionalization of monolithic and porous three-dimensional graphene by one-step chitosan electrodeposition for enzymatic biosensor, ACS Appl. Mater. Interfaces 6 (2014) 19997.
[16] J. Yang, E. Zhang, X. Li, Y. Yu, J. Qu, Z.-Z. Yu, Direct reduction of graphene oxide by Ni foam as a high-capacitance supercapacitor electrode, ACS Appl. Mater. Interfaces 8 (2016) 2297.
[17] Z. Chen, W. Ren, L. Gao, B. Liu, S. Pei, H.-M. Cheng, Three-dimensional flexible and conductive interconnected graphene networks grown by chemical vapour deposition, Nat. Mater. 10 (2011) 424.

[18] S. He, W. Chen, 3D graphene nanomaterials for binder-free supercapacitors: scientific design for enhanced performance, Nanoscale 7 (2015) 6957.
[19] Y. Gu, H. Wu, Z. Xiong, W.A. Abdulla, X.S. Zhao, The electrocapacitive properties of hierarchical porous reduced graphene oxide templated by hydrophobic $CaCO_3$ spheres, J. Mater. Chem. A 2 (2014) 451.
[20] X. Zhang, D. Liu, L. Yang, L. Zhou, T. You, Self-assembled three-dimensional graphene-based materials for dye adsorption and catalysis, J. Mater. Chem. A 3 (2015) 10031.
[21] K. Liu, Y.M. Chen, G.M. Policastro, M.L. Becker, Y. Zhu, Three-dimensional Bicontinuous graphene monolith from polymer templates, ACS Nano 9 (2015) 6041.
[22] Q. Fang, X. Zhou, W. Deng, Z. Liu, Ordered self-assembly of amphipathic graphene nanosheets into three-dimensional layered architectures, Nanoscale 8 (2016) 197.
[23] B. Yu, D. Kuang, S. Liu, C. Liu, T. Zhang, Template-assisted self-assembly method to prepared three-dimensional reduced graphene oxide for dopamine sensing, Sens. Actuators B 205 (2014) 120.
[24] M. Kota, X. Yu, S.-H. Yeon, H.-W. Cheong, H.S. Park, Ice-templated three dimensional nitrogen doped graphene for enhanced supercapacitor performance, J. Power Sources 303 (2016) 372.
[25] X. Feng, Y. Zhang, J. Zhou, Y. Li, S. Chen, L. Zhang, Y. Ma, L. Wang, X. Yan, Three-dimensional nitrogen-doped graphene as an ultrasensitive electrochemical sensor for the detection of dopamine, Nanoscale 7 (2015) 2427.
[26] B.J. Gross, R.V. Branchflower, T.R. Burke, D.E. Lees, L.R. Pohl, Bone marrow toxicity in vitro of chloramphenicol and its metabolites, Toxicol. Appl. Pharmacol. 64 (1982) 557.
[27] J.C. Hanekamp, A. Bast, Antibiotics exposure and health risks: chloramphenicol, Environ. Toxicol. Pharmacol. 39 (2015) 213.
[28] Q.Q. Zhang, G.G. Ying, C.G. Pan, Y.S. Liu, J.L. Zhao, Comprehensive evaluation of *anti*biotics emission and fate in the river basins of China: source analysis, multimedia modeling, and linkage to bacterial resistance, Environ. Sci. Technol. 49 (2015) 6772.
[29] J.A. Turton, C.M. Andrews, A.C. Havard, T.C. Williams, Studies on the haemotoxicity of chloramphenicol succinate in the dunkin hartley guinea pig, Int. J. Exp. Pathol. 83 (2002) 225.
[30] G. Liu, C. Chai, Towards the development of a sensitive electrochemical sensor for the determination of chloramphenicol residues in milk, Anal. Methods 7 (2015) 1572.
[31] C.H. Kim, L.P. Lee, J.R. Min, M.W. Lim, S.H. Jeong, An indirect competitive assay-based aptasensor for detection of oxytetracycline in milk, Biosens. Bioelectron. 51 (2014) 426.
[32] A. Azzouz, E. Ballesteros, Multiresidue method for the determination of pharmacologically active substances in egg and honey using a continuous solid-phase extraction system and gas chromatography-mass spectrometry, Food Chem. 178 (2015) 63–69.
[33] T. Sniegocki, A. Posyniak, M. Gbylik-Sikorska, J. Zmudzki, Determination of chloramphenicol in milk using a quechers-based on liquid chromatography tandem mass spectrometry method, Anal. Lett. 47 (2014) 568.
[34] H.Y. Shen, H.L. Jiang, Screening, determination and confirmation of chloramphenicol in seafood, meat and honey using ELISA, HPLC-UVD, GC-ECD, GC–MS-EI-SIM and GCMS-NCI-SIM Methods, Anal. Chim. Acta 535 (2005) 33–41.
[35] L. Vera-Candiotia, A.C. Olivieri, H.C. Goicoechea, Development of a novel strategy for preconcentration of antibiotic residues in milk and their quantitation by capillary electrophoresis, Talanta 82 (2010) 213.
[36] W. Ji, W. Yao, Rapid surface enhanced raman scattering detection method for chloramphenicol residues, Spectrochim. Acta A 144 (2015) 125.
[37] K. Xu, Y. Sun, W. Li, J. Xu, B. Cao, Y. Jiang, T. Zheng, J. Li, D. Pan, Multiplex chemiluminescent immunoassay for screening of mycotoxins using photonic crystal microsphere suspension array, Analyst 139 (2014) 771.
[38] F. Xiao, F.Q. Zhao, J.W. Li, R. Yan, J.J. Yu, B.Z. Zeng, Sensitive voltammetric determination of chloramphenicol by using single-wall carbon nanotube-gold nanoparticle-ionic liquid composite film modified glassy carbon electrodes, Anal. Chim. Acta 596 (2007) 79.
[39] G. Yang, F. Zhao, Electrochemical sensor for chloramphenicol based on novel multiwalled carbon nanotubes@molecularly imprinted polymer, Biosens. Bioelectron. 64 (2015) 416.
[40] F. Ricci, G. Volpe, L. Micheli, G. Palleschi, A review on novel developments and applications of immunosensors in food analysis, Anal. Chim. Acta 605 (2007) 111.
[41] R.R. Yang, J.L. Zhao, M.J. Chen, T. Yang, S.Z. Luo, K. Jiao, Electrocatalytic determination of chloramphenicol based on molybdenum disulfide nanosheets and self-doped polyaniline, Talanta 131 (2015) 619.
[42] J. Borowiec, R. Wang, L. Zhu, J. Zhang, Synthesis of nitrogen-doped graphene nanosheets decorated with gold nanoparticles as an improved sensor for electrochemical determination of chloramphenicol, Electrochim. Acta 99 (2013) 138.
[43] F.Y. Kong, T.T. Chen, J.Y. Wang, H.L. Fang, D.H. Fan, W. Wang, UV-assisted synthesis of tetrapods-like titanium nitride-reduced graphene oxide nanohybrids for electrochemical determination of chloramphenicol, Sens. Actuators B 225 (2016) 298.
[44] Z.D. Yan, N. Gan, T.H. Li, Y.T. Cao, Y.J. Chen, A sensitive electrochemical aptasensor for multiplex antibiotics detection based on high-capacity magnetic hollow porous nanotracers coupling exonuclease-assisted cascade target recycling, Biosens. Bioelectron. 78 (2016) 51.
[45] H. Zhai, Z. Liang, Z. Chen, H. Wang, Z. Liu, Z. Su, Q. Zhou, Simultaneous detection of metronidazole and chloramphenicol by differential pulse stripping voltammetry using a silver nanoparticles/sulfonate functionalized graphene modified glassy carbon electrode, Electrochim. Acta 171 (2015) 105.
[46] R.N. Rosy Goyal, Y.B. Shim, Glutaraldehyde sandwiched amino functionalized polymer based aptasensor for the determination and quantification of chloramphenicol, RSC Adv. 5 (2015) 69356.
[47] X. Zhang, Y.C. Zhang, L.X. Ma, One-pot facile fabrication of graphene-zinc oxide composite and its enhanced sensitivity for simultaneous electrochemical detection of ascorbic acid, dopamine and uric acid, Sens. Actuator B 227 (2016) 488.
[48] J.W.S. Hummers, R.E. Offeman, Preparation of graphitic oxide, J. Am. Chem. Soc. 80 (1958) 1339.
[49] X. Zhang, B. Zhang, D.Y. Liu, J.L. Qiao, One-pot synthesis of ternary alloy CuFePt nanoparticles anchored on reduced graphene oxide and their enhanced electrocatalytic activity for both methanol and formic acid oxidation reactions, Electrochim. Acta 177 (2015) 93.
[50] S.F. Pei, J.P. Zhao, J.H. Du, W.C. Ren, H.M. Cheng, Direct reduction of graphene oxide films into highly conductive and flexible graphene films by hydrohalic acids, Carbon 48 (2010) 4466.
[51] J. Lu, I. Do, L.T. Drzal, R.M. Worden, I. Lee, Nanometal-Decorated Exfoliated Graphite nanoplatelet based Glucose Biosensors with High Sensitivity and Fast Response, ACS Nano (2) (2008) 1825.
[52] X. Zhang, L.X. Ma, Y.C. Zhang, Electrodeposition of platinum nanosheets on C_{60} decorated glassy carbon electrode as a stable electrochemical biosensor for simultaneous detection of ascorbic acid, dopamine and uric acid, Electrochim. Acta 177 (2015) 118.
[53] X. Chen, Y. Wang, J. Zhou, W. Yan, X. Li, J.J. Zhu, Electrochemical impedance immunosensor based on three-dimensionally ordered macroporous gold film, Anal. Chem. 80 (2008) 2133.
[54] A.J. Bard, L.R. Faulkner, Electrochemical Methods: Fundamentals Applications, 2nd ed, John Wiley & Sons Inc, New York, 2001.
[55] T. Yang, H. Chen, T. Ge, J. Wang, W. Li, K. Jiao, Highly sensitive determination of chloramphenicol based on thin-layered MoS_2/polyaniline nanocomposite, Talanta 144 (2015) 1324.